

Beam collimation in the Main Injector *

B.C. Brown, A.I. Drozhdin

Fermi National Accelerator Laboratory

P.O. Box 500, Batavia, Illinois 60510

November 22, 2004

1 Collimation in the Main Injector

A very high beam power (~ 0.13 MW) of the beam injected from the 8 GeV Linac into the Main Injector and tight aperture defined by the extraction and injection Lambertson magnets (Table 1) as well as a complicated set of orbit bumps (Table 2 and 3) during the cycle implies serious constraints on beam losses in the machine. All eight straight sections of the Main Injector are occupied by the RF cavities, injection and extraction systems. The horizontal orbit bumps (Fig. 1 and 2) used for a closed orbit displacement at the Lambertson magnet septa do not permit to install horizontal collimators close to the beam in the straight sections occupied by the extraction and injection systems. The only straight sections which can be used for a beam collimation are MI22 for vertical and MI-30 for horizontal collimation of the beam (Figs. 3 and 4). Currently a kicker-magnet is located at the center of MI-30 which is used both for a beam extraction from the MI to the Recycler and for injection from the Recycler to the MI. Additionally to this a horizontal closed orbit bump (Fig. 5) is used for a kicked beam displacement reduction in the region from MI-22 to MI-32. To resolve this conflict the primary and secondary collimators will be retracted from the accelerator aperture at those cycles which are used for the antiproton beam recycling.

Another complication is that dispersion is equal to zero at all straight sections of accelerator. This requires to place off-momentum primary collimator in the arc preceding the MI30 straight section. The vertical primary collimator is necessary to place in the arc preceding the MI22 straight section to get required phase advance between primary and secondary collimators.

1.1 Collimation System Parameters

A possible location of a two-stage collimation system is shown in Figs. 3, 4 and 6. The system consists of one primary and two secondary collimators both for horizontal and vertical planes. Secondary collimators are located in an optimal phase advance downstream of the primary collimators. This provides the halo particles collimation at the secondary collimators during the first turn after interaction with the primary one. Assuming that 5% of the beam is collimated at injection and 0.5% at the top energy this amount 16 kW of power intercepted by the secondary collimators. Simulations show that this power is intercepted mostly by the two secondary collimators with about 5-10 kW per each of them. This requires local steel shielding of ~ 2.5 m long which extends to ~ 1 m transversely around the secondary collimators and the first quadrupole downstream of the collimator.

*Work supported by the Universities Research Association, Inc., under contract DE-AC02-76CH03000 with the U. S. Department of Energy.

The horizontal secondary collimators are located at the first half-cell of the MI30. This leaves the rest 3.5 cells for the electron cooling and new RF system.

The mechanical design of the secondary collimators and targets will be similar to those already built and installed in the Tevatron for Collider Run II. Those collimators consist of 2 pieces of stainless steel, 0.5 m long, welded together in an L-shape configuration (Fig. 7). The collimator assembly is welded inside a stainless steel box with bellows on each end. Full range of motion is 50 mm in steps as small as $25 \mu\text{m}$ if required and a maximum speed of 2.5 mm/sec. Position readback is provided by linear differential voltage transformers. The primary collimator assembly is identical to the collimator assembly except that the target L-shape blocks are only 0.1 m in length. The 1 mm thick machined tungsten primary collimator jaws are bolted to the stainless steel blocks. The blocks provide a good heat sink for energy dissipated in the tungsten. The entire assembly, including bellows, will occupy approximately 0.6 m of lattice space.

A total of 16 kW of DC power can be removed from a single collimator by circulating standard LCW (Low Conductivity Water) through cooling channels on the outside of the collimator box. A flow of 3 gpm will remove this power with a temperature rise of 20°C .

2 Simulations of Beam Loss at Collimation System Operation

At normal operating conditions, a circulating beam size grows slowly with a small step size per turn. A corresponding proton impact parameter on a collimator would be of the order of few μm . A thin primary collimator increases proton amplitude as a result of multiple Coulomb scattering and thus results in drastic increase of impact parameter from $\sim 10 \mu\text{m}$ at the primary collimator to $\sim 1 \text{ mm}$ at the secondary collimators. This results in a significant reduction of the out-scattered proton yield and total beam loss in the accelerator, decreases collimator jaw overheating and mitigates requirements on the collimator alignment [2].

A multi-turn particle tracking through the accelerator with halo interactions with the collimators is conducted with the STRUCT code [3]. All the accelerator components with their real strengths and aperture restrictions are taken into account. The β -functions, dispersions and phase advances at the collimators are presented in Table 5. The 1-mm thick tungsten primary collimators are positioned at the edge of the beam after painting injection ($40\pi \text{ mm} \cdot \text{mrad}$) both in vertical and horizontal planes. The secondary collimator jaws are located with 2 mm offset from the primary ones. The proton beam position at injection and at 120 GeV with respect to the primary and secondary collimators are shown in Fig. 8. At the top energy the circulating beam orbit is moved closer to the collimators edge by the vertical correctors V217, V219, V221, V223 and V225 at MI22, and by the horizontal correctors H228, H230, H302 and H304 at MI30 straight section. Fig. 8 represents position of $162\pi \text{ mm} \cdot \text{mrad}$ beam at the top energy. The size of $162\pi \text{ mm} \cdot \text{mrad}$ beam at 120 GeV is equal to the size of $12\pi \text{ mm} \cdot \text{mrad}$ beam at injection. The numerical simulations are done for the Main Injector [1] in the presence of orbit displacement during the cycle, Lambertson magnets aperture limitations and aperture restrictions presented at Tables 1 - 4. The proton beam position at injection and at 120 GeV with respect to the Lambertson magnet septa are shown in Fig. 9. As shown here, the circulating beam is pretty close to the septum of Lambertson magnet at MI60 and at MI40.

Horizontal and vertical phase space at injection in the primary and secondary collimators are presented in Fig. 10 with 1 mm thick tungsten primary collimator. Large amplitude protons are intercepted by the secondary collimators during the first turn after interaction with the primary collimator. Protons with amplitudes smaller than secondary collimators position survive during several tens of turns until they increase amplitude in the next interactions with primary collimators. These particles produce a secondary halo and occupy the $(40\pi \text{ mm} \cdot \text{mrad} + 2 \text{ mm})$ envelope. The

phase spaces at the collimators with 0.5 mm and 0.2 mm thick tungsten primary collimators are shown in Fig. 11 and 12.

Beam loss distributions at injection around the accelerator and in the collimation region are shown in Figures 13, 14 and 15 for different thickness of primary collimator. Accelerator intensity is assumed to be equal to 1.5×10^{14} *ppp*, repetition rate is 0.67 Hz, and 5% of total intensity is assumed to be lost at injection at these simulations. The losses behind primary collimators are an order of magnitude less with thin (0.2 mm) primary collimator compared to the thick (1 mm) one.

Beam loss distributions at 120 GeV around the accelerator and in the collimation region are shown in Figures 16, 17 and 18 for different strength of collimation bumps. 0.5% of total intensity is assumed to be lost at 120 GeV at these simulations. Beam losses at the Lambertson magnets of MI60 and MI40 are very big for the large emittance beam ($162\pi mm \cdot mrad$) compared to the small one ($54\pi mm \cdot mrad$). This means that the circulating beam should be kept close to the collimators during the entire cycle.

3 Conclusions

A two-stage beam halo collimation system located at MI22 and MI30 has been proposed. The system consists of 0.5-mm thick tungsten primary collimators positioned at the edge of the beam after painting injection ($40\pi mm \cdot mrad$) both in vertical and horizontal planes. The secondary collimator jaws are located with 2 mm offset from the primary ones. Horizontal and vertical bumps are used to keep the edge of the circulating beam close to the collimator jaws during the accelerator cycle.

At collimation of 5% of total intensity at injection and 0.5% at the top energy beam losses in the collimation region at injection are 20 W/m and at 120 GeV - 10 W/m. In the rest part of accelerator they are 1-10 W/m at injection and 1 W/m at the top energy with several peaks exceeding this level by a factor of 10 (MI60) and 100 (MI40, MI52).

References

- [1] Main Injector Technical Design Handbook, Fermilab, November 1995
- [2] "The proton driver design study", Fermilab-TM-2136, December 2000.
- [3] I. Baishev, A. Drozhdin, and N. Mokhov, 'STRUCT Program User's Reference Manual', SSCL-MAN-0034 (1994), <http://www-ap.fnal.gov/~drozhdin/>

name	location	septa position		rotation
		horizontal	vertical	
		mm	mm	
LAM60A entr	MI-60	2.0	-1.5	0.145
LAM60A exit	MI-60	2.0	-1.5	0.145
LAM60B entr	MI-60	2.0	-1.5	0.020
LAM60B exit	MI-60	2.0	-1.5	0.020
LAM60C entr	MI-60	2.0	0.0	0.000
LAM60C exit	MI-60	2.0	0.0	0.000
LAM62C entr	MI-62	5.0	0.0	0.037
LAM62C exit	MI-62	5.0	0.0	0.037
LAM62B entr	MI-62	4.0	-3.0	0.098
LAM62B exit	MI-62	4.0	-3.0	0.098
LAM62A entr	MI-62	2.0	-4.0	0.220
LAM62A exit	MI-62	2.0	-4.0	0.220
LAM10 entr	MI-10	0.0	7.5	0.043633
LAM10 exit	MI-10	0.0	7.5	0.043633
LAM222 entr	MI-22	-5.0	0.0	0.000
LAM222 exit	MI-22	-5.0	0.0	0.000
LAM321 entr	MI-32	12.0	0.0	0.000
LAM321 exit	MI-32	12.0	0.0	0.000
LAM40A entr	MI-40	-2.0	-3.0	0.220
LAM40A exit	MI-40	-2.0	-3.0	0.220
LAM40B entr	MI-40	-1.0	0.0	0.108
LAM40B exit	MI-40	-1.0	0.0	0.108
LAM40C entr	MI-40	2.5	-2.0	0.070
LAM40C exit	MI-40	2.5	-2.0	0.070
LAM52A entr	MI-52	2.0	-3.0	0.220
LAM52A exit	MI-52	2.0	-3.0	0.220
LAM52B entr	MI-52	7.0	-1.0	0.098
LAM52B exit	MI-52	7.0	-1.0	0.098
LAM52C entr	MI-52	7.5	-1.0	0.037
LAM52C exit	MI-52	7.5	-1.0	0.037

Table 1: Lambertson magnets position and aperture. Entrance and exit are related to the proton direction.

name	location	horizontal	vertical
		mm	mm
IQB210	Q602	1.13	0.0
IQB075	Q606	-1.403	0.0
IQD026	Q610	-1.22	0.0
IQD041	Q612	0.042	0.0
IQB046	Q614	1.10	0.0
IQD029	Q618	-3.232	0.0
IQE134	Q620	0.306	0.0
IQC024	Q622	-3.257	0.0
IQD006	Q641	0.0	0.0
IQG333	Q101	0.0	0.0
IQB176	Q103	0.0	0.0
IQD010	Q218	0.0	0.0
IQC023	Q220	0.0	0.0
IQB045	Q222	0.0	0.0
IQC009	Q319	0.0	0.0
IQB071	Q321	0.0	0.0
IQD037	Q323	0.0	0.0
IQD015	Q340	-0.688	0.0
IQC035	Q400	-3.078	0.0
IQE065	Q402	-0.919	0.0
IQC036	Q404	-3.041	0.0
IQD043	Q406	0.0	0.0
IQD016	Q518	-0.531	0.0
IQC022	Q520	-2.377	0.0
IQE072	Q522	-0.710	0.0
IQD024	Q524	-2.398	0.0
IQD018	Q526	-0.329	0.0

Table 2: Main quadrupoles displacement.

name	location	length	B injection	B 120 GeV	system
		m	kG	kG	
H602	Q602	0.3048	-0.094980	0.0	extraction to NuMI
H606	Q606	0.3048	0.122380	0.0	
H610	Q610	0.3048	0.140912	0.0	
H612	Q612	0.3048	-0.003609	0.0	
H614	Q614	0.3048	-0.097277	0.0	
H618	Q618	0.3048	0.243483	0.0	antiproton extraction
H620	Q620	0.3048	-0.015496	0.0	
H622	Q622	0.3048	0.206837	0.0	
V641	Q641	0.3048	0.454612	1.914167	proton injection
V101	Q101	0.3048	-0.113542	-0.478074	
V103	Q103	0.3048	0.476582	2.006673	
V217	Q217	0.3048	0.0	-2.18	vertical collimation
V219	Q217	0.3048	0.0	-1.45	
V221	Q223	0.3048	0.0	0.387	
V223	Q223	0.3048	0.0	-1.32592	
V225	Q225	0.3048	0.0	2.74535	
H220	Q220	0.3048	-0.376349	-2.580411	antiproton extraction to recycler
H222	Q222	0.3048	0.033086	0.226854	
H224	Q224	0.3048	-0.428911	-2.940797	
H224	Q224	0.3048	0.628655	0.0	Kick compensation
H226	Q226	0.3048	0.186812	0.0	
H304	Q304	0.3048	1.037037	0.0	
H318	Q318	0.3048	-0.158234	0.0	
H320	Q320	0.3048	-0.499033	0.0	
H228	Q228	0.3048	0.0	1.581	horizontal collimation
H230	Q230	0.3048	0.0	-1.054	
H302	Q302	0.3048	0.0	-1.088515	
H304	Q304	0.3048	0.0	-1.35648	
H320	Q320	0.3048	0.258827	2.65	antiproton injection from recycler
H322	Q322	0.3048	0.005413	0.055421	
H324	Q324	0.3048	0.360555	3.691542	
H340	Q340	0.3048	0.0	0.0	beam abort
H400	Q400	0.3048	0.223720	0.0	
H402	Q402	0.3048	0.014799	0.0	
H404	Q404	0.3048	0.219101	0.0	
H406	Q406	0.3048	0.0	0.0	
H518	Q518	0.3048	0.0	0.0	proton extraction and antiproton injection
H520	Q520	0.3048	0.231776	0.0	
H522	Q522	0.3048	-0.024367	0.0	
H524	Q524	0.3048	0.262963	0.0	
H526	Q526	0.3048	0.0	0.0	

Table 3: Corretor strength at injection and at 120 GeV.

name	horizontal half-size	vertical half-size
	mm	mm
elliptical aperture main dipoles and quadrupoles	61.35	26.54
rectangular aperture collimators	40.	40.
rectangular aperture foil	6.	6.
elliptical aperture Q100	26.54	61.35
round aperture LALAM222, M321	38.5	38.5
cross type aperture Q402, Q522, Q608, Q620	63.0	29.0

Table 4: Main Injector aperture in the calculations.

Table 5: β -functions, dispersion and phase advances between collimators.

element	β -functions, m	dispersion, m	Phase advance between primary and secondary collimators, degree	
			horizontal	vertical
	hor. / ver.			
vert. prim. PrV.	11.21/41.38	0.21	-	0
secondary V1	51.65/16.07	0.17	-	45
secondary V2	14.17/49.67	-0.08	-	162
horiz. prim. PrH.	37.58/ 7.91	1.42	0	-
secondary H1	14.68/51.62	0.08	158	-
secondary H2	50.50/14.20	2.54	185	-

Table 6: Horizontal and vertical position of collimators.

element	envelope of circulating beam (3σ), mm respect to beam pipe center, mm				collimator position with	
	horizontal		vertical		horizontal	vertical
	injection	top energy	injection	top energy		
vert. prim. PrV.	6.888	1.872	13.299	3.599	-8.90	-14.18
secondary V1	14.775	4.019	8.265	2.241	-16.90	-9.97
secondary V2	7.737	2.104	14.517	3.942	19.70	16.39
horiz. prim. PrH.	12.600	3.428	5.742	1.573	-11.88	7.80
secondary H1	7.878	2.143	14.778	4.019	8.58	16.90
secondary H2	14.604	3.974	7.716	2.109	15.42	-9.90

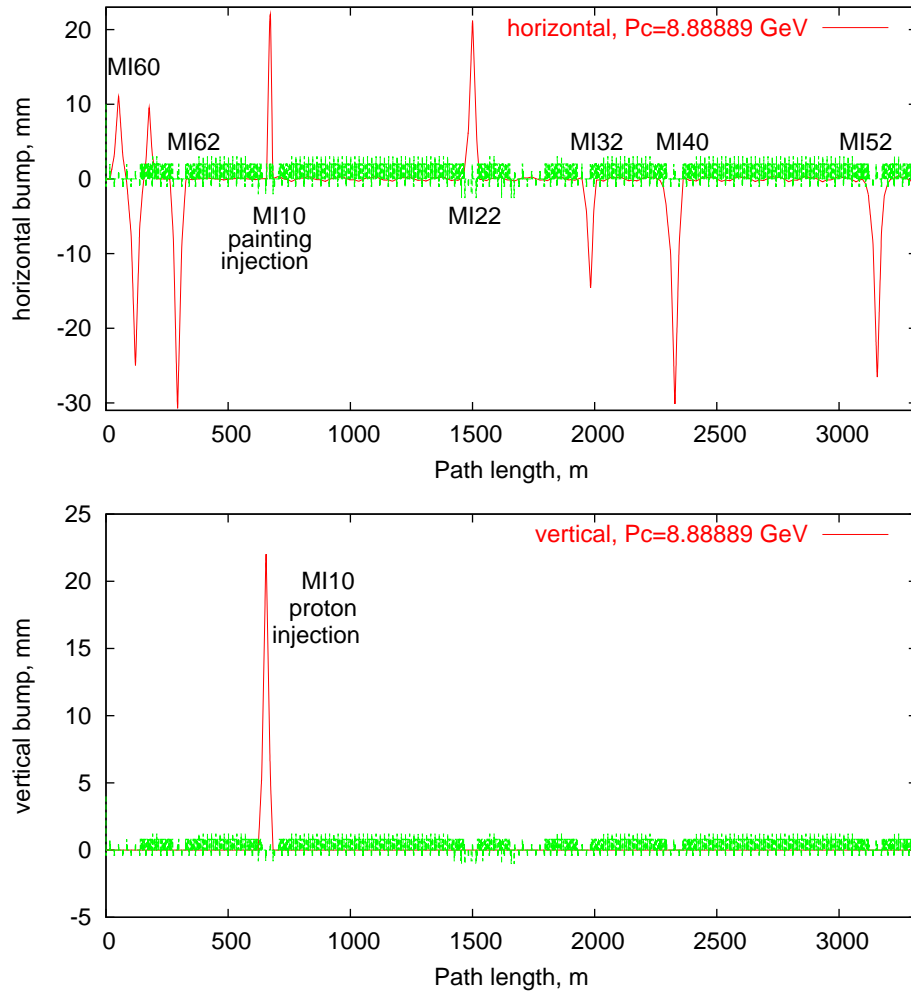


Figure 1: Horizontal (top) and vertical (bottom) orbit at injection in the Main Injector.

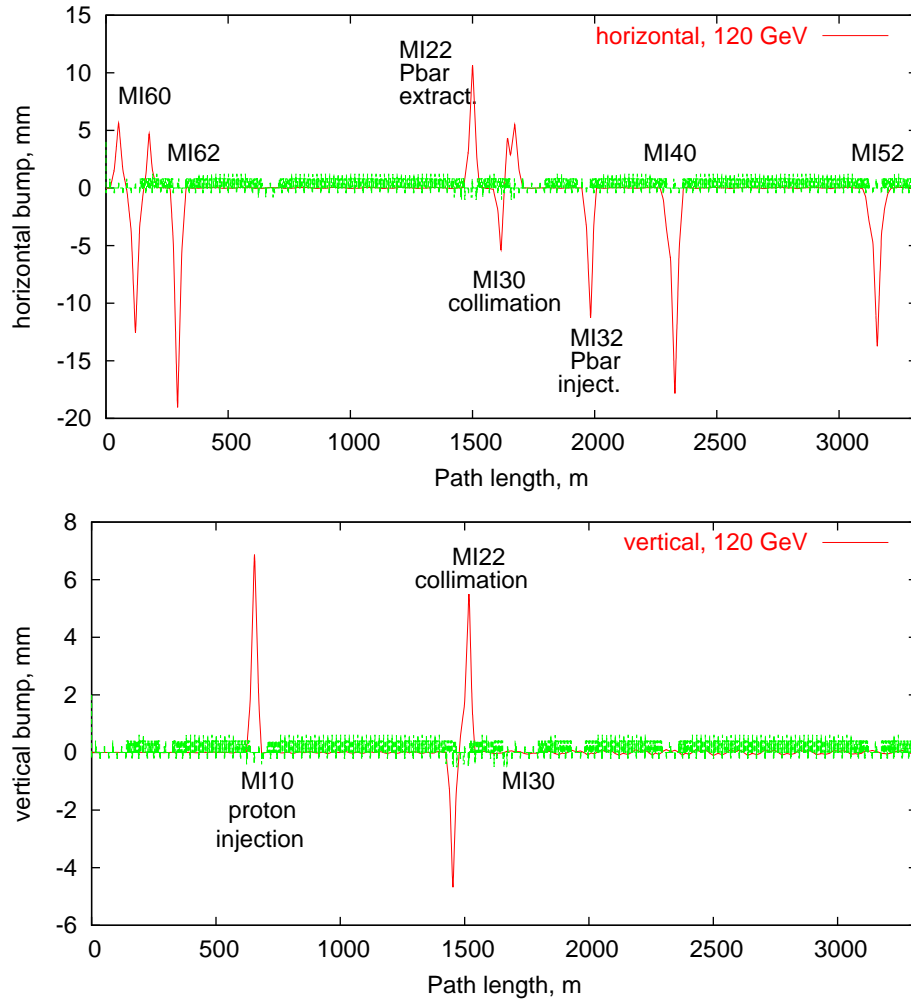


Figure 2: Horizontal (top) and vertical (bottom) orbit at 120 GeV in the Main Injector.

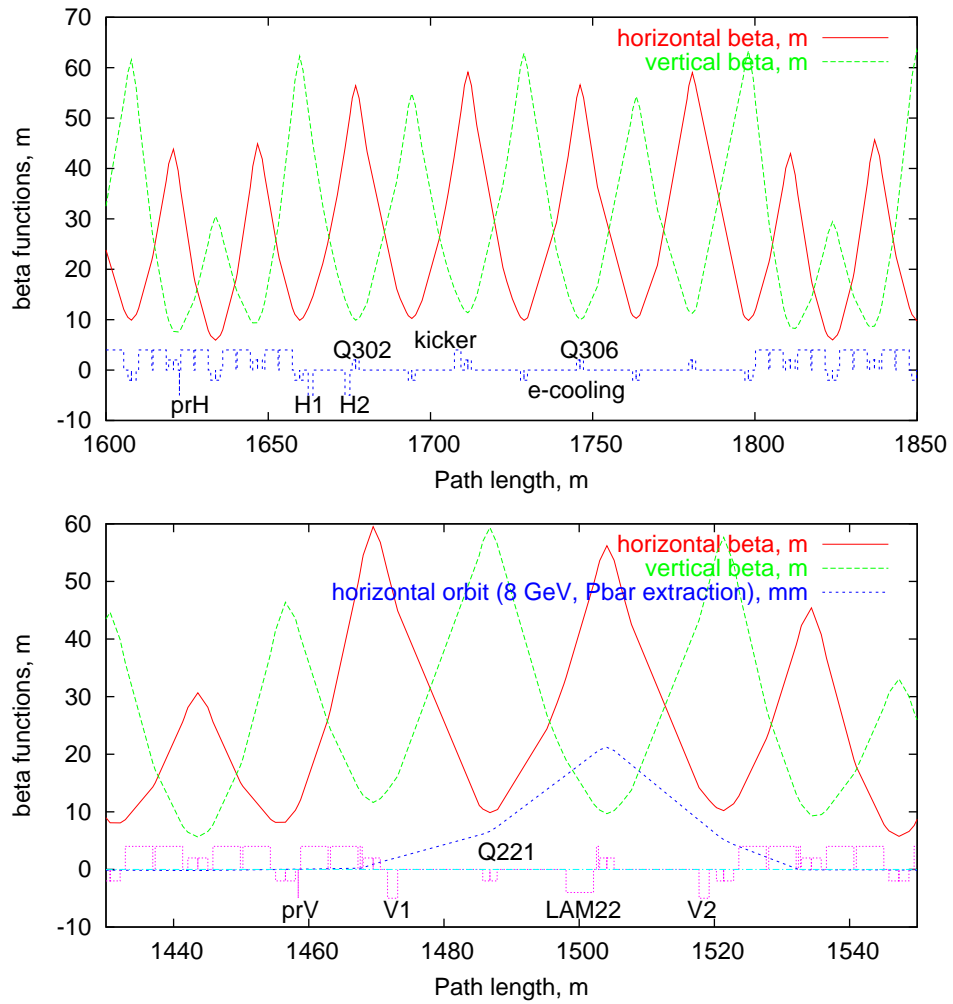


Figure 3: Horizontal (top) and vertical (bottom) collimation at MI30 and MI22 sections of the Main Injector.

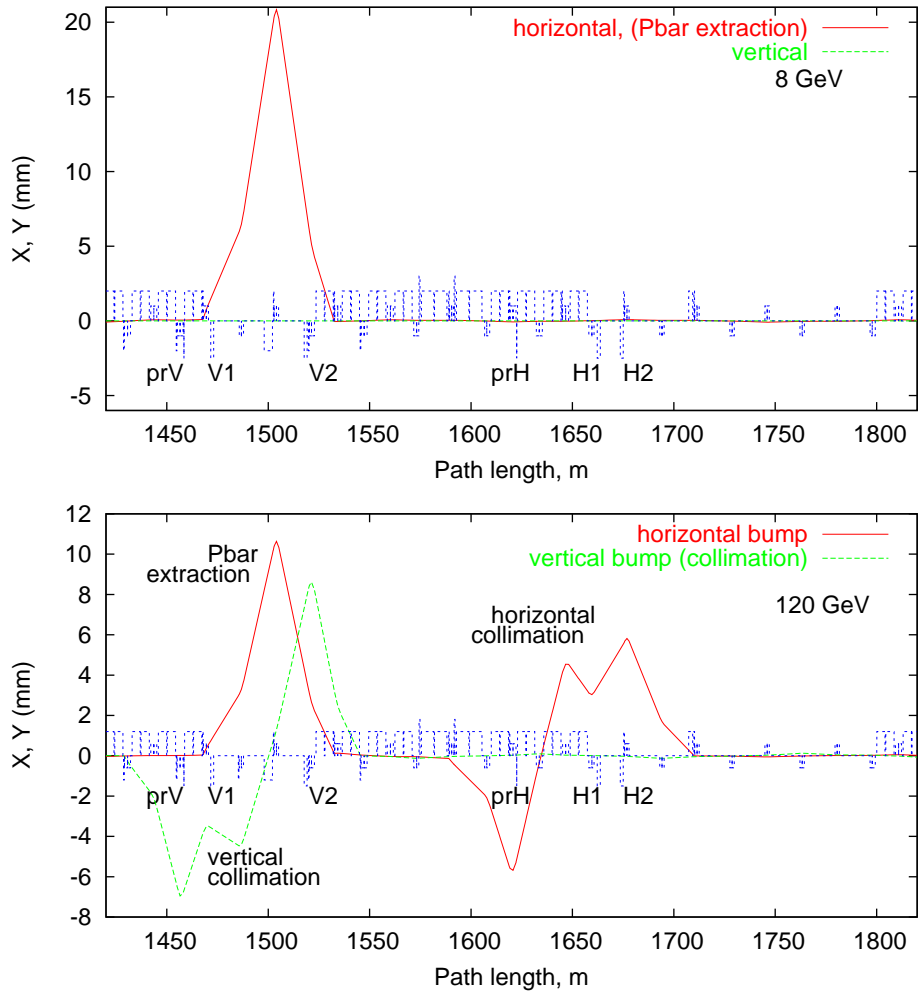


Figure 4: Horizontal and vertical beam orbits at injection (top) and at 120 GeV (bottom) in the collimation region (MI22 and MI30) of the Main Injector.

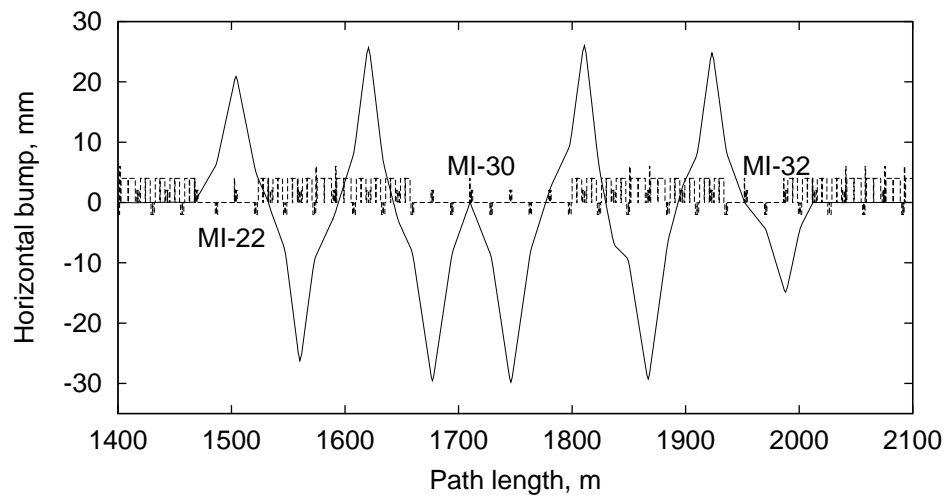


Figure 5: Horizontal closed orbit bump used for a kicked beam displacement reduction in the MI-30 section and beam displacement at the injection and extraction Lambertson magnets at MI-22 and MI-32.

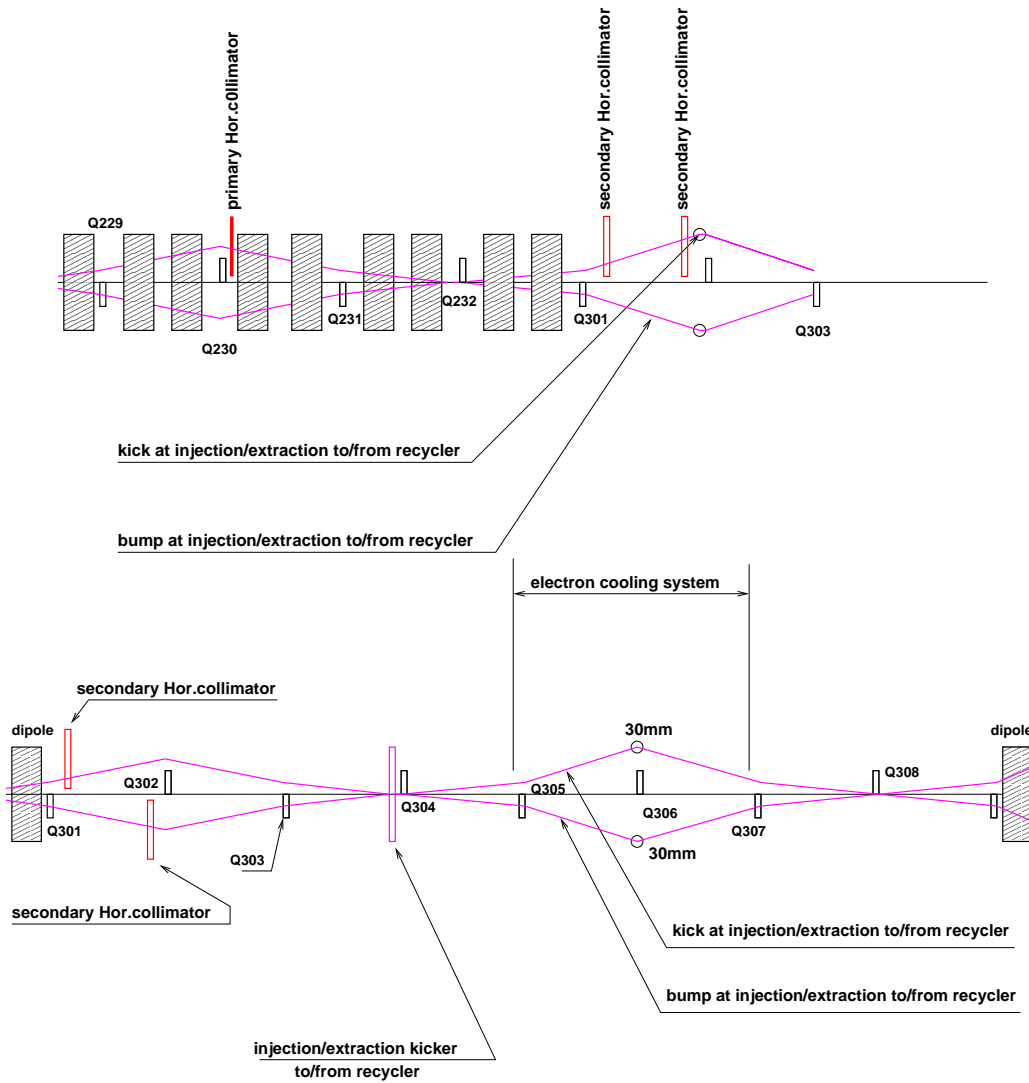


Figure 6: Location of horizontal collimation system in MI30 section of the Main Injector. Horizontal primary collimator is located in the arc preceding the MI-30 straight section in a region with dispersion $D=1.4$ m. Secondary collimators are in the optimal phase advances with respect to the primary one.

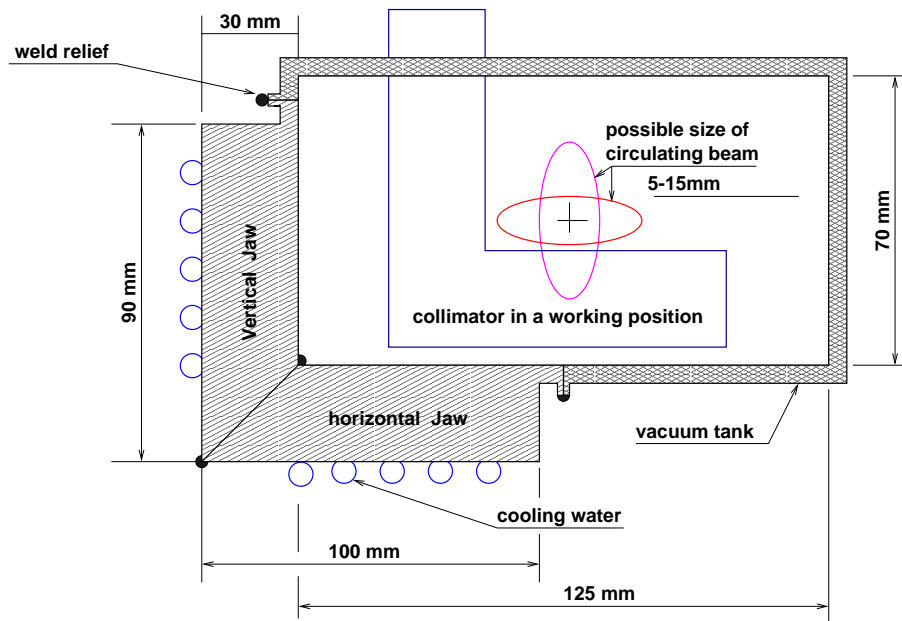


Figure 7: Secondary collimator cross section.

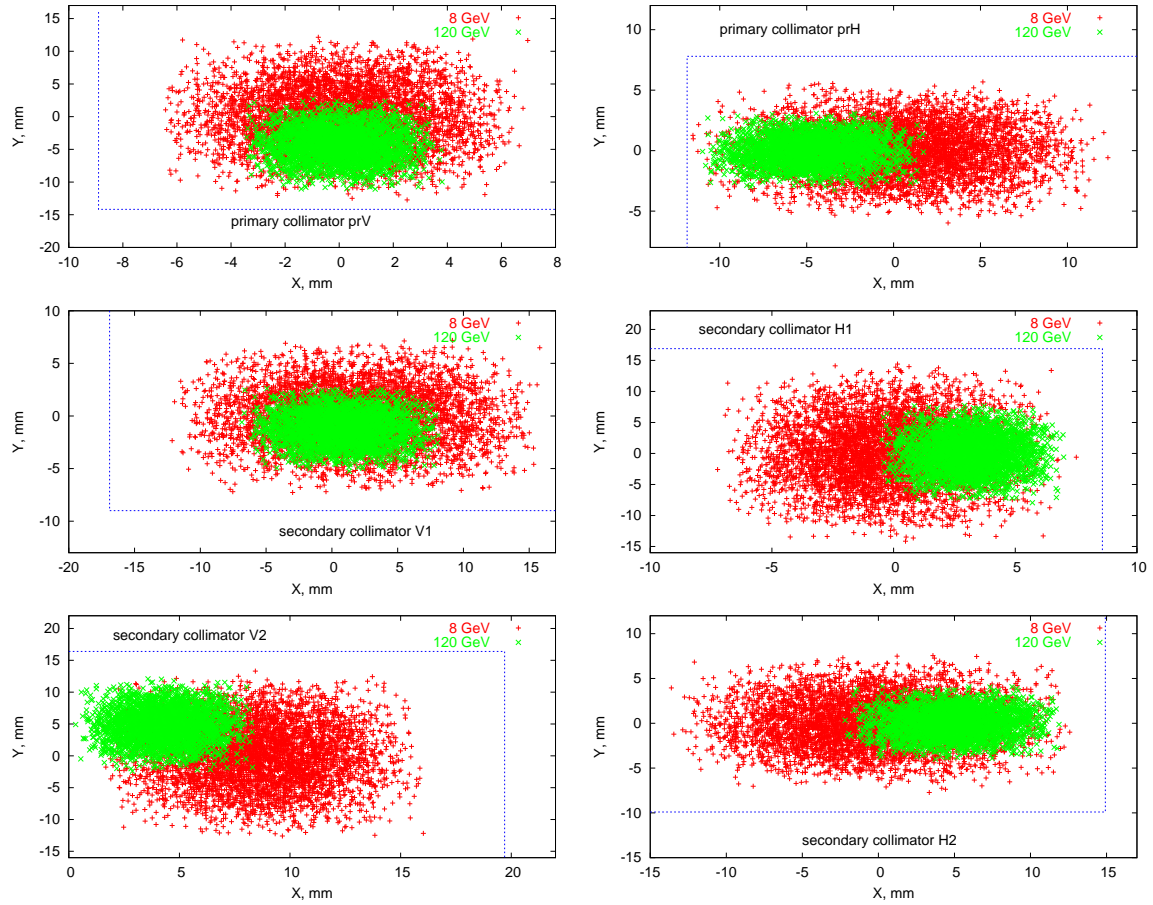


Figure 8: The proton beam position at injection and at 120 GeV with respect to the vertical (left) and horizontal (right) primary and secondary collimators. The $162\pi\text{mm} \cdot \text{mrad}$ beam is shown at 120 GeV. The beam size of $162\pi\text{mm} \cdot \text{mrad}$ beam at 120 GeV is equal to the size of $12\pi\text{mm} \cdot \text{mrad}$ beam at injection.

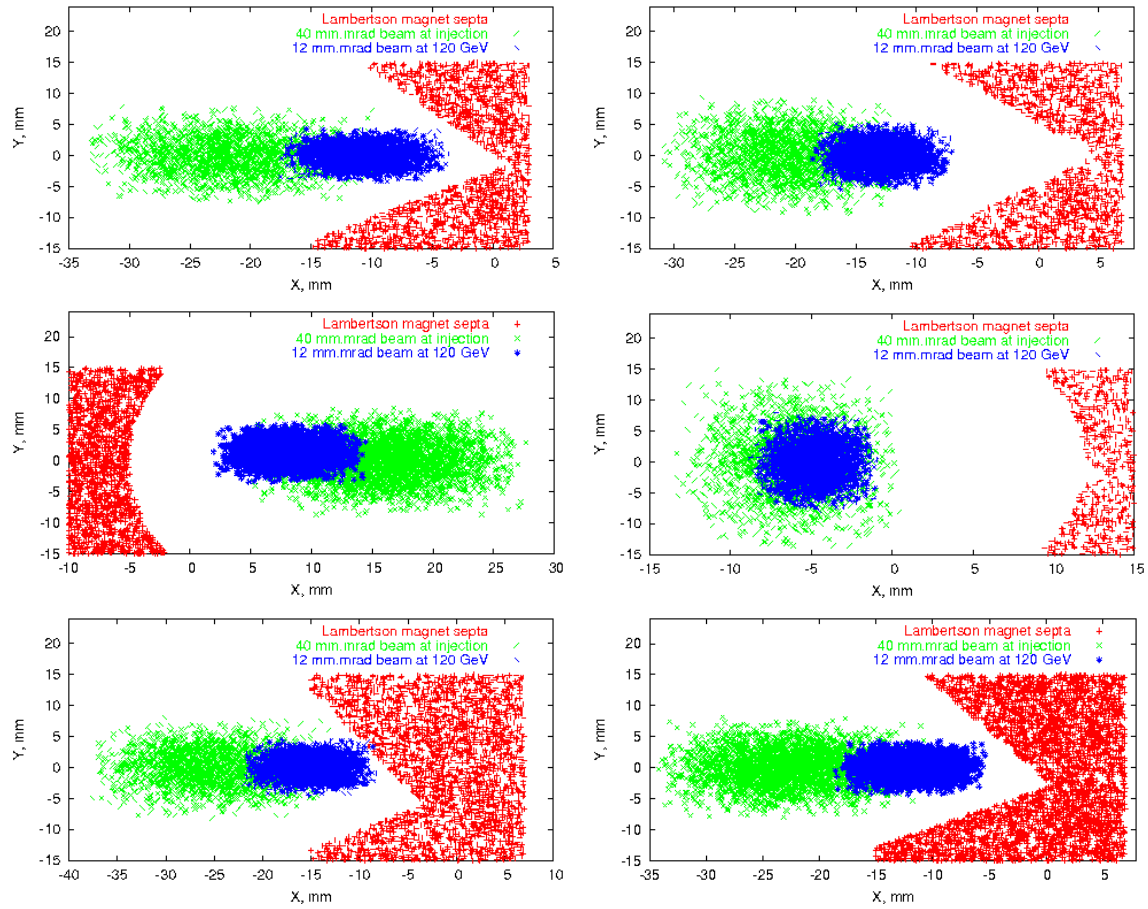


Figure 9: Circulating beam position at injection and at 120 GeV with respect to the Lambertson magnet septa at MI60 (top, left), MI62 (top, right), MI22 (middle, left), MI32 (middle, right), MI40 (bottom, left), MI52 (bottom, right). The $162\pi\text{mm}\cdot\text{mrad}$ beam is shown at 120 GeV.

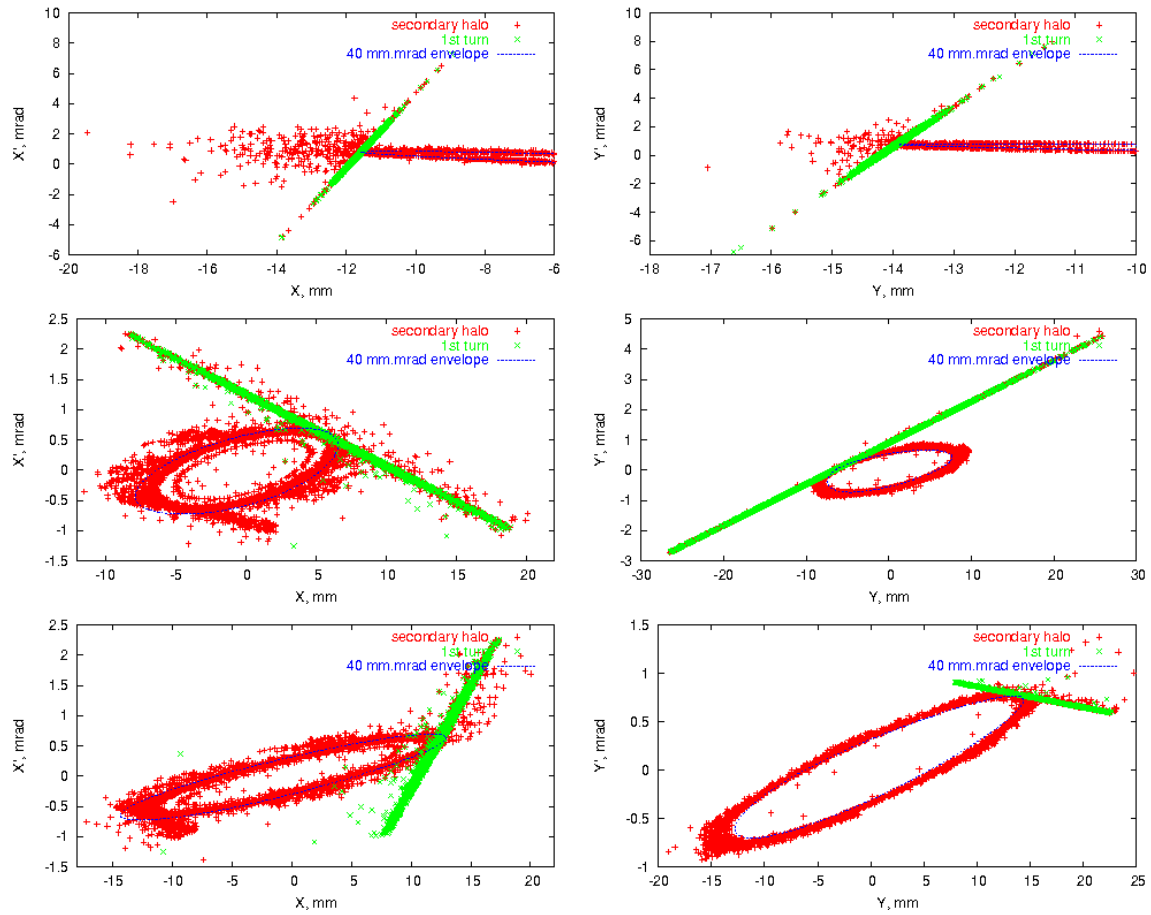


Figure 10: Horizontal (left) and vertical (right) phase space at injection at primary collimators (top), secondary collimator No.1 (middle) and No.2 (bottom) with 1 mm thick tungsten primary collimators. Green (grey) – halo particles at the first turn after interaction with the primary collimator, red (black) – secondary halo, blue (black line) – $40\pi \text{ mm} \cdot \text{mrad}$ envelope.

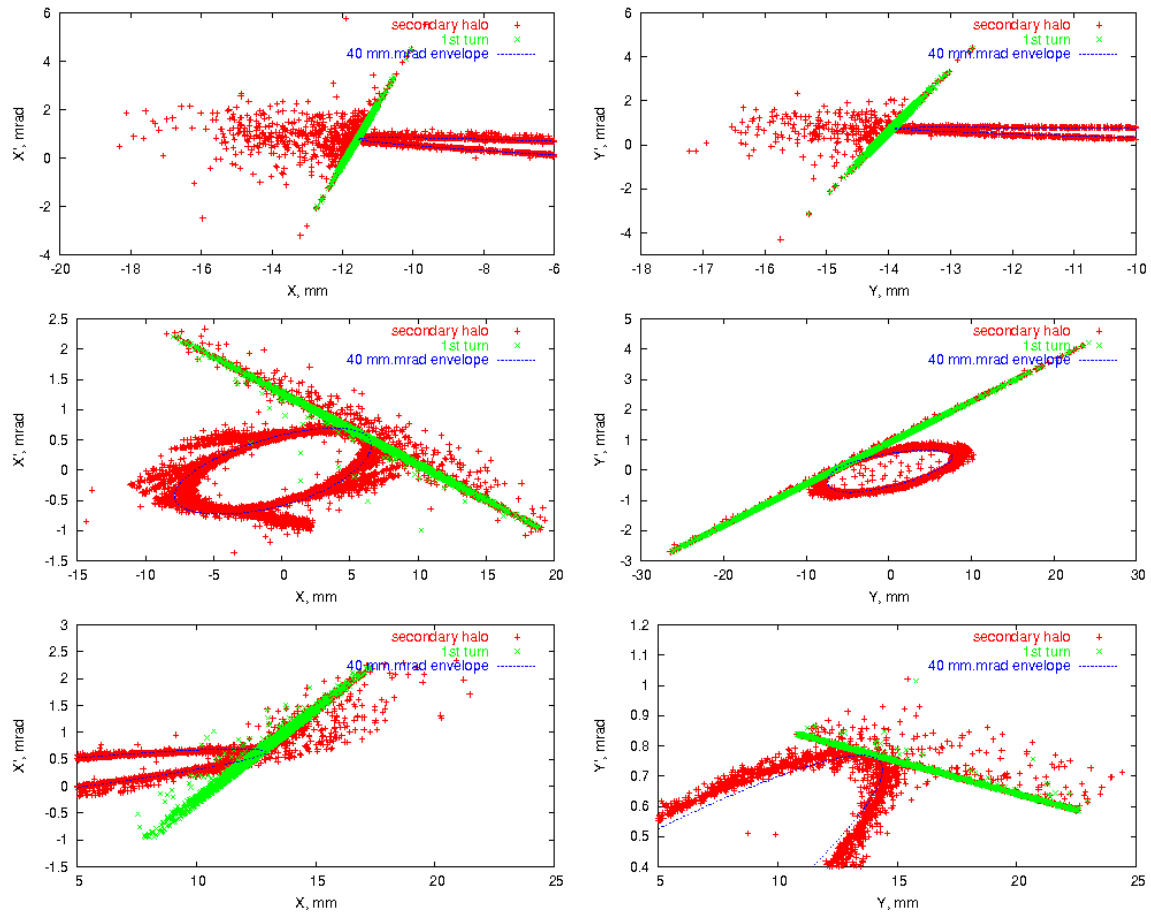


Figure 11: Horizontal (left) and vertical (right) phase space at injection at primary collimators (top), secondary collimator No.1 (middle) and No.2 (bottom) with 0.5 mm thick tungsten primary collimators. Green (grey) – halo particles at the first turn after interaction with the primary collimator, red (black) – secondary halo, blue (black line) – $40\pi \text{ mm} \cdot \text{mrad}$ envelope.

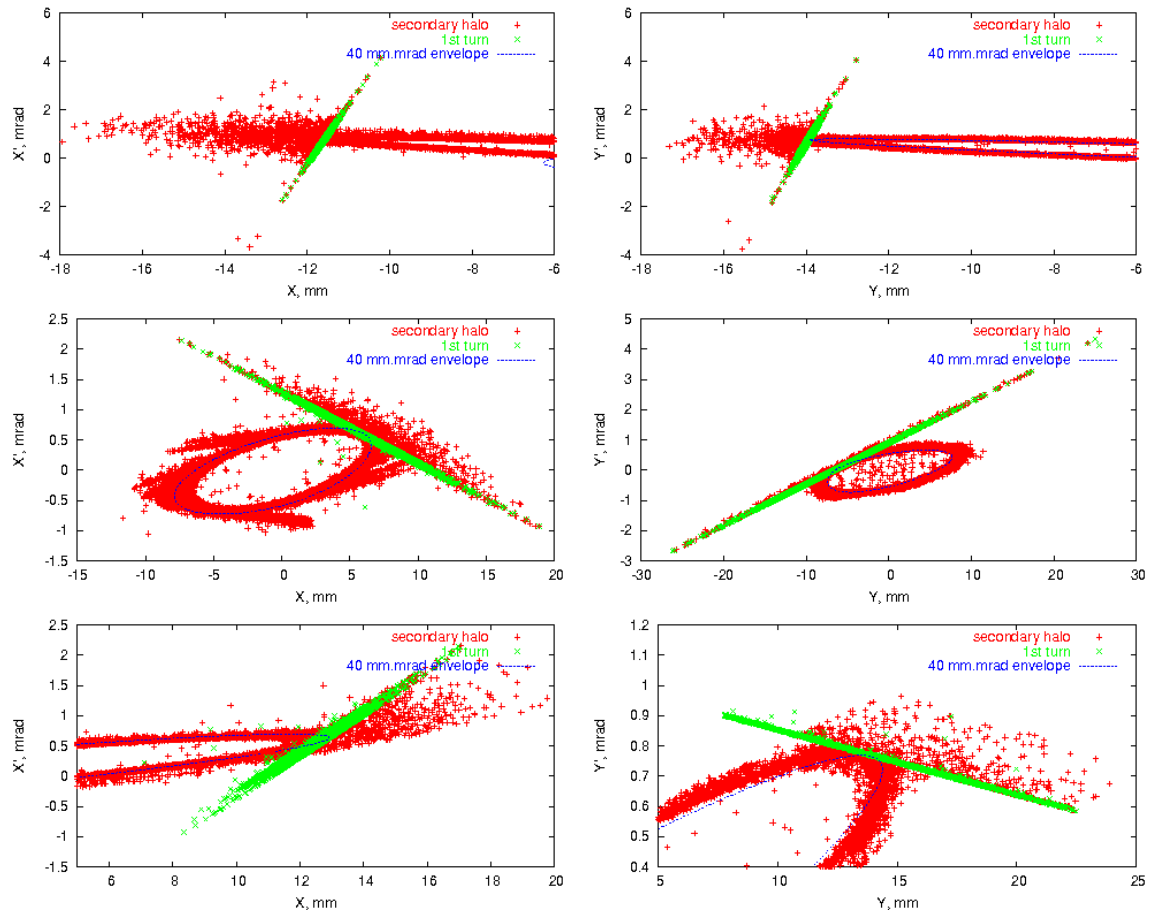


Figure 12: Horizontal (left) and vertical (right) phase space at injection at primary collimators (top), secondary collimator No.1 (middle) and No.2 (bottom) with 0.2 mm thick tungsten primary collimators. Green (grey) – halo particles at the first turn after interaction with the primary collimator, red (black) – secondary halo, blue (black line) – $40\pi \text{ mm} \cdot \text{mrad}$ envelope.

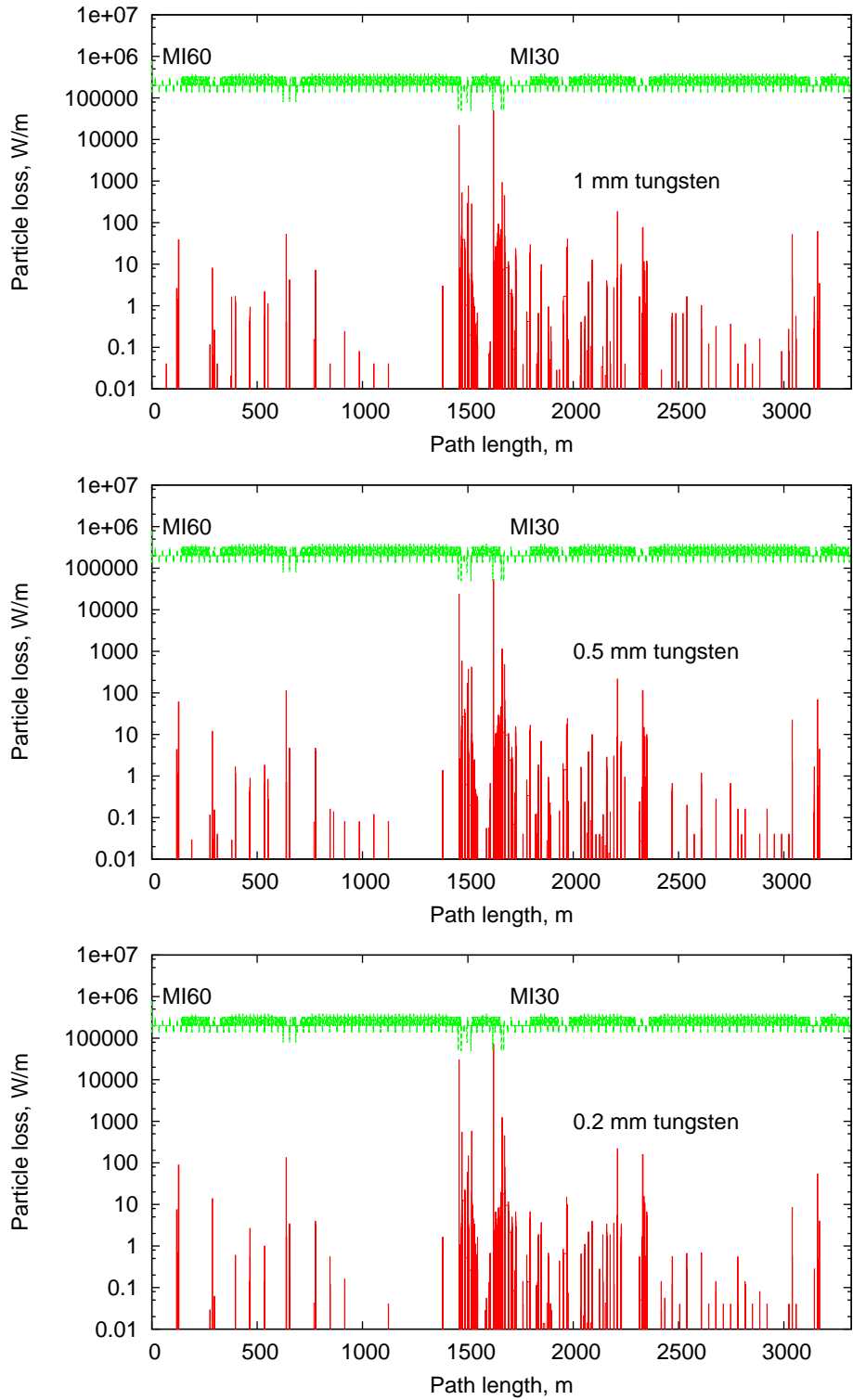


Figure 13: Beam loss at injection with 1 mm (top), 0.5 mm (middle) and 0.2 mm (bottom) thick tungsten primary collimators. Injected intensity is 1.5×10^{14} *ppp*, repetition rate is 0.67 Hz. 5% of total intensity is assumed lost at injection.

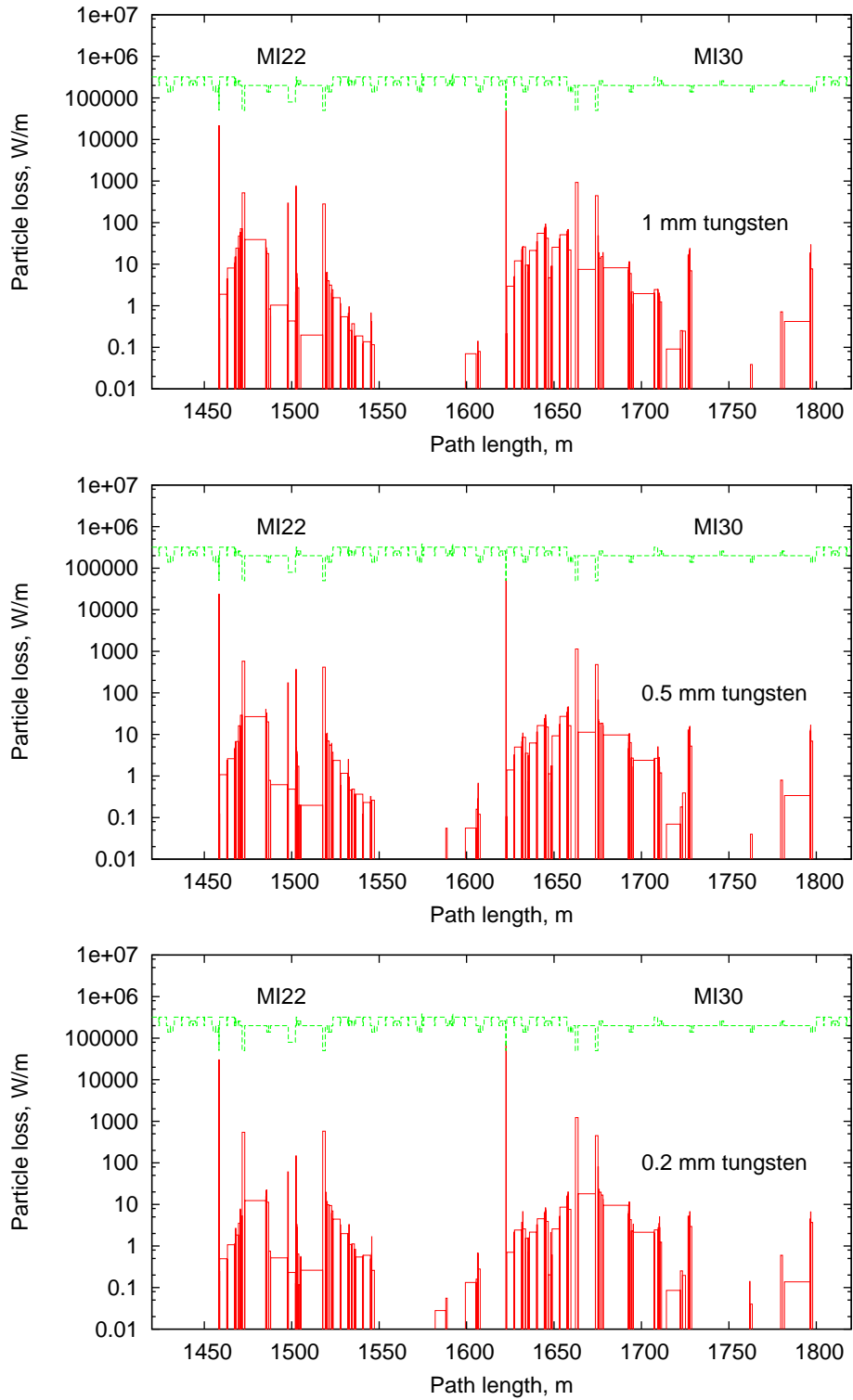


Figure 14: Beam loss distribution at injection with 1 mm (top), 0.5 mm (middle) and 0.2 mm (bottom) thick tungsten primary collimators in the collimation region (MI22 and MI30). Injected intensity is 1.5×10^{14} *ppp*, repetition rate is 0.67 Hz. 5% of total intensity is assumed lost at injection.

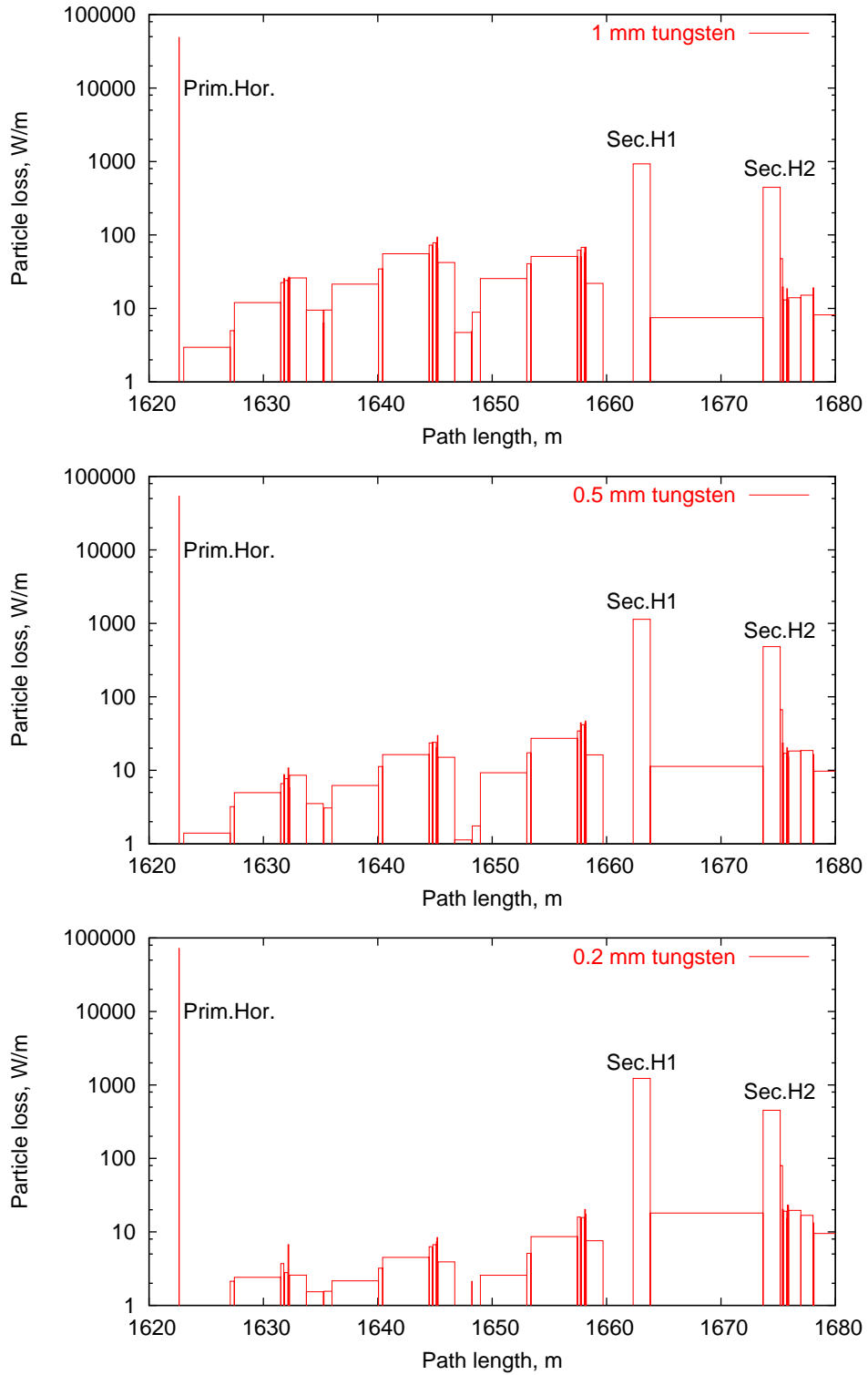


Figure 15: Beam loss at MI30 region at injection with 1 mm (top), 0.5 mm (middle) and 0.2 mm (bottom) thick tungsten primary collimators. Injected intensity is 1.5×10^{14} *ppp*, repetition rate is 0.67 Hz. 5% of total intensity is assumed lost at injection.

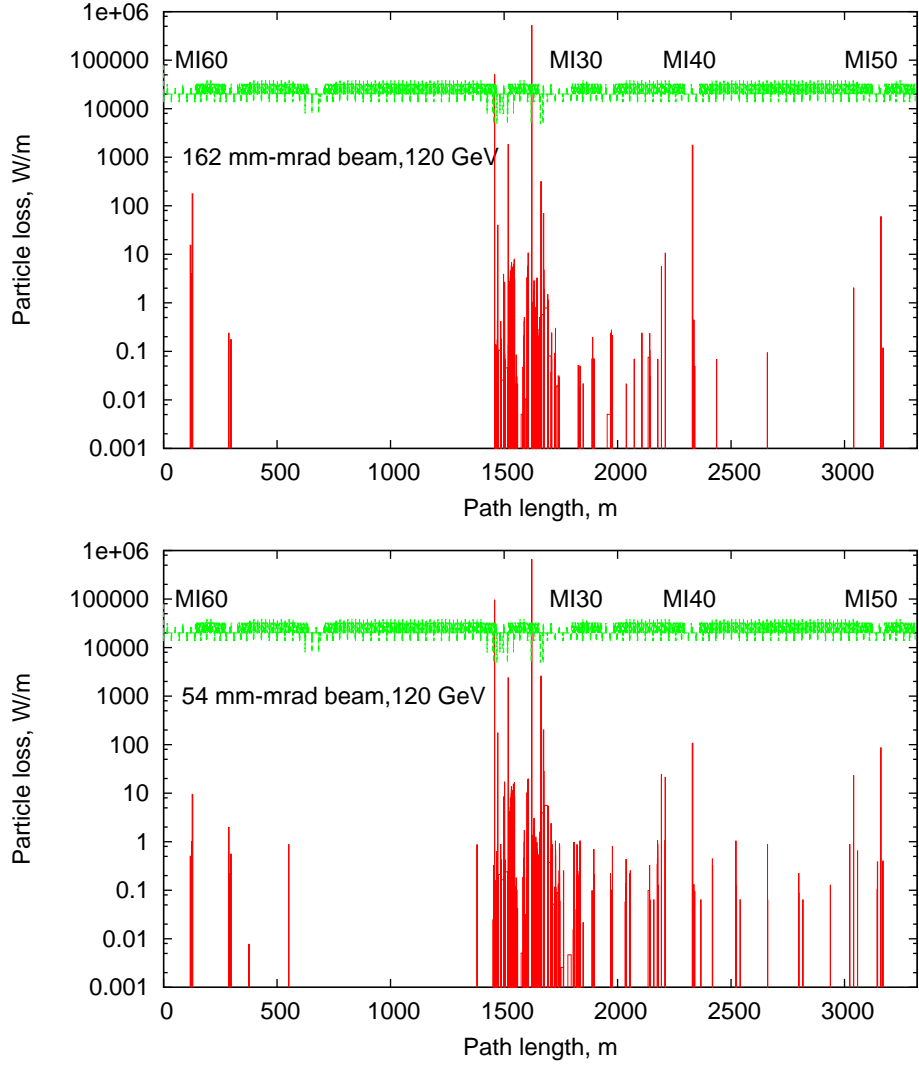


Figure 16: Beam loss at 120 GeV with 0.5 mm thick tungsten primary collimators. Top - collimation bump bring 162π beam edge to the primary and secondary collimators, bottom - bump bring 54π beam to the collimators. Beam size of 162π beam at 120 GeV is equal to 12π beam at injection, beam size of 54π beam at 120 GeV is equal to 4π beam at injection. Intensity is 1.5×10^{14} *ppp*, repetition rate is 0.67 Hz. 0.5% of total intensity is assumed lost at 120 GeV.

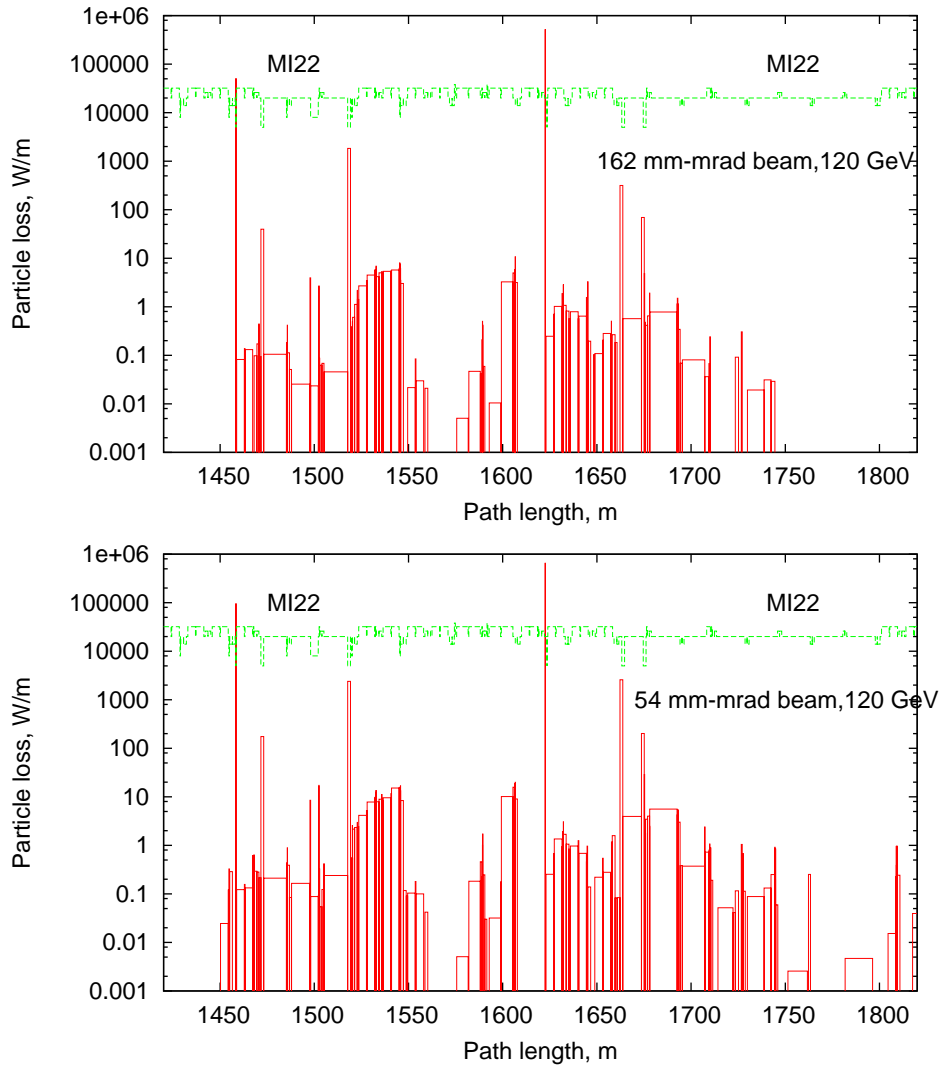


Figure 17: Beam loss in the collimation region (MI22 and MI30) at 120 GeV with 0.5 mm thick tungsten primary collimators. Top - collimation bump bring 162π beam edge to the primary and secondary collimators, bottom - bump bring 54π beam to the collimators. Beam size of 162π beam at 120 GeV is equal to 12π beam at injection, beam size of 54π beam at 120 GeV is equal to 4π beam at injection. Intensity is 1.5×10^{14} ppp, repetition rate is 0.67 Hz. 0.5% of total intensity is assumed lost at 120 GeV.

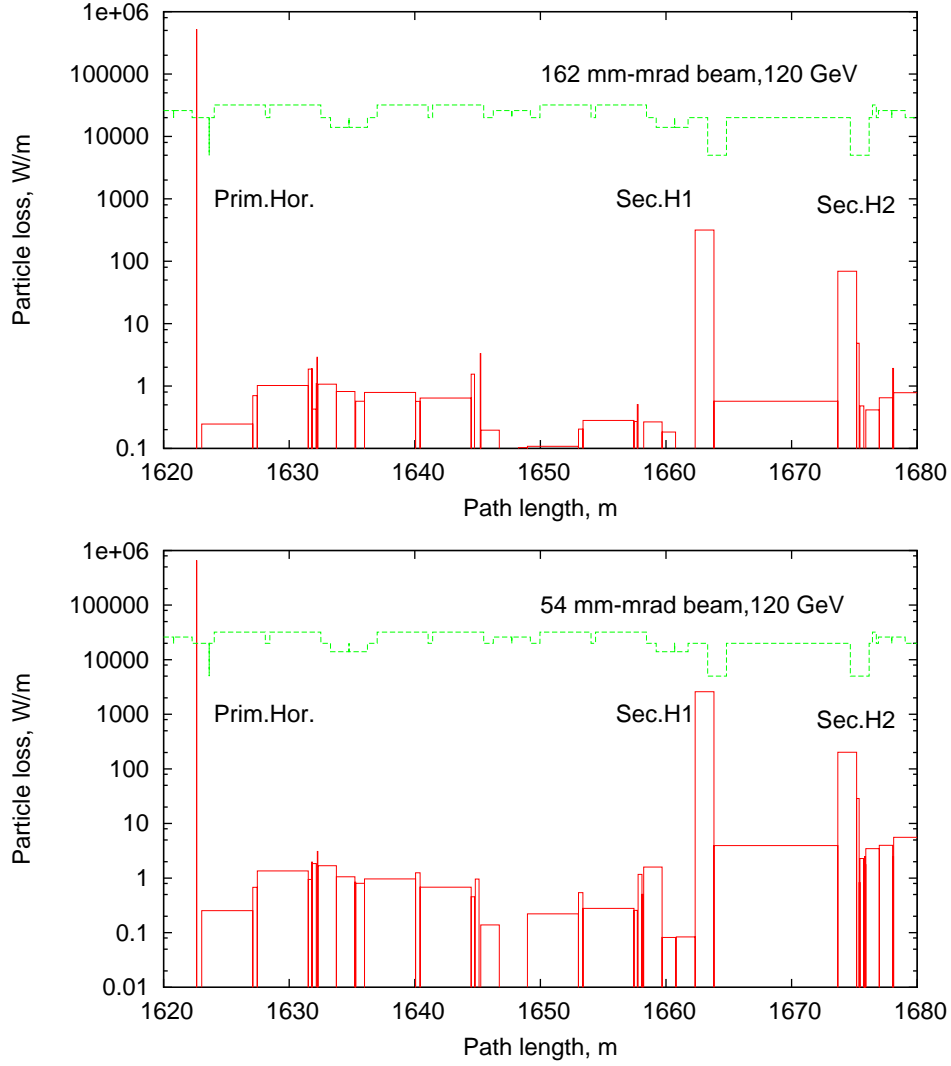


Figure 18: Beam loss at MI30 at 120 GeV with 0.5 mm thick tungsten primary collimators. Top - collimation bump bring 162π beam edge to the primary and secondary collimators, bottom - bump bring 54π beam to the collimators. Beam size of 162π beam at 120 GeV is equal to 12π beam at injection, beam size of 54π beam at 120 GeV is equal to 4π beam at injection. Intensity is 1.5×10^{14} *ppp*, repetition rate is 0.67 Hz. 0.5% of total intensity is assumed lost at 120 GeV.